BIOCHEMISTRY
including biophysical chemistry & molecular biology

Article

pubs.acs.org/biochemistry

Peptoid-Substituted Hybrid Antimicrobial Peptide Derived from Papiliocin and Magainin 2 with Enhanced Bacterial Selectivity and Anti-inflammatory Activity

Areum Shin,[†] Eunjung Lee,[†] Dasom Jeon,[†] Young-Guen Park,[†] Jeong Kyu Bang,[‡] Yong-Sun Park,[§] Song Yub Shin,[∥] and Yangmee Kim*[,†]

[†]Department of Bioscience and Biotechnology, Konkuk University, Hwayang-dong, Gwangjin-gu, Seoul 143-701, Korea

[‡]Division of Magnetic Resonance, Korea Basic Science Institute, 804-1 Yangchung-ri, Ochang, Chungbuk 363-883, Republic of Korea

[§]Department of Chemistry, Konkuk University, Hwayang-dong, Gwangjin-gu, Seoul 143-701, Korea

[∥]Department of Bio-Materials, Graduate School, and Department of Cellular and Molecular Medicine, School of Medicine, Chosun University, Gwangju 501-759, Republic of Korea

Supporting Information

ABSTRACT: Antimicrobial peptides (AMPs) are important components of the host innate immune system. Papiliocin is a 37-residue AMP purified from larvae of the swallowtail butterfly *Papilio xuthus*. Magainin 2 is a 23-residue AMP purified from the skin of the African clawed frog *Xenopus laevis*. We designed an 18-residue hybrid peptide (PapMA) incorporating N-terminal residues 1−8 of papiliocin and N-terminal residues 4−12 of magainin 2, joined by a proline (Pro) hinge. PapMA showed high antimicrobial activity but was cytotoxic to mammalian cells. To decrease PapMA cytotoxicity, we designed a lysine (Lys) peptoid analogue, PapMA-k, which retained high antimicrobial activity but displayed cytotoxicity lower than that of PapMA. Fluorescent dye leakage experiments and confocal microscopy showed that PapMA targeted bacterial cell membranes whereas PapMA-k penetrated bacterial cell membranes. Nuclear magnetic resonance experiments revealed that PapMA contained an N-terminal α-helix from Lys^3 to Lys^7 and a C-terminal α-helix from Lys^{10} to Lys^{17}, with a Pro^9 hinge between them. PapMA-k also had two α-helical structures in the same region connected with a flexible hinge residue at $Nlys^9$, which existed in a dynamic equilibrium of *cis* and *trans* conformers. Using lipopolysaccharide-stimulated RAW264.7 macrophages, the anti-inflammatory activity of PapMA and PapMA-k was confirmed by inhibition of nitric oxide and inflammatory cytokine production. In addition, treatment with PapMA and PapMA-k decreased the level of ultraviolet irradiation-induced expression of genes encoding matrix metalloproteinase-1 (MMP-1), interleukin-6 (IL-6), and tumor necrosis factor-α (TNF-α) in human keratinocyte HaCaT cells. Thus, PapMA and PapMA-k are potent peptide antibiotics with antimicrobial and anti-inflammatory activity, with PapMA-k displaying enhanced bacterial selectivity.

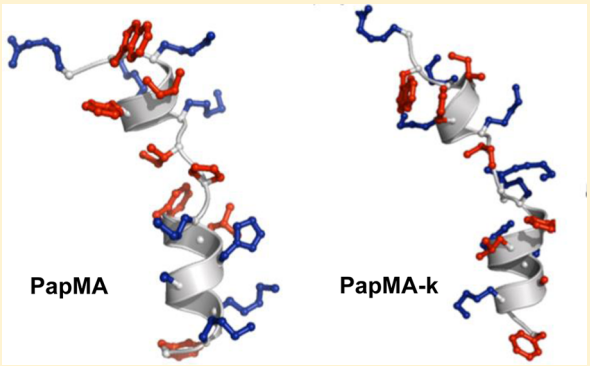

Antimicrobial peptides (AMPs) are produced by organisms ranging from insects to humans and play an essential role in innate immunity.[1−3] In recent years, the emergence of antibiotic-resistant bacterial strains has resulted in a search for new antibiotics.[1−4] AMPs have emerged as novel therapeutic alternatives to traditional antibiotics.[1−4] The bactericidal mechanism of AMPs is different from that of existing antibiotics.[5−9] Although the precise mechanism underlying AMP function has not been fully elucidated, it appears to involve depolarization or permeabilization of the bacterial cell membrane.[5−9]

Papiliocin is a 37-residue AMP found in larvae of the swallowtail butterfly (*Papilio xuthus*).[10] We reported that papiliocin has high antimicrobial activity against Gram-negative bacteria and high anti-inflammatory activity and antifungal activity.[10−13] The bactericidal and fungicidal mechanisms involve disruption of bacterial and fungal cell membranes, respectively.[11−13] The tertiary structure of papiliocin was determined by nuclear magnetic resonance (NMR) spectroscopy.[13] Papiliocin has an amphipathic N-terminal helix and a hydrophobic C-terminal helix. Trp^2 and Phe^5 at the N-terminal helix are key residues that interact with cell membranes of Gram-negative bacteria.[13] Magainin 2 is a 23-residue AMP isolated from the skin of the African clawed frog (*Xenopus laevis*). Magainin 2 displays high antimicrobial activity against both Gram-negative bacteria and Gram-positive bacteria without cytotoxic effects against mammalian cells.[14,15]

Received: April 14, 2015
Revised: June 8, 2015
Published: June 8, 2015

DOI: 10.1021/acs.biochem.5b00392
Biochemistry 2015, 54, 3921−3931

Hybrid AMPs have been constructed by combining the active regions of two maternal AMPs. We designed these hybrid peptides to increase antimicrobial activity and reduce cytotoxicity against mammalian cells.[16−21] In our previous paper, cecropin A (CA)−magainin 2 (MA) hybrid peptides were designed, and the structure−function relationships of CAMA hybrid peptides were investigated. CAMA showed high antimicrobial activity without toxicity against human erythrocytes.[17,18,20,21] We designed CAMA analogues featuring a GIG deletion or a substitution of GIG with Pro.[20,21] The Pro-substituted CAMA analogue displayed improved antimicrobial and anticancer activity with low cytotoxicity, suggesting the hinge region was a key determinant associated with hybrid AMP function.[21] Moreover, the P18 analogue of CAMA inhibits inflammatory responses by LPS-stimulated macrophages.[21]

There are several AMPs that contain a Pro residue as a hinge in the central region of the structure.[20−23] Pro has distinctive properties, as it lacks a backbone amide proton to act as a hydrogen bond donor and has a restricted torsional conformational space, resulting in a break in the $i-i+4$ hydrogen bond formed in an α-helical structure.[24,25] Similar to Pro, peptoid residues have an ability to form a β-turn and to break an α-helical structure.[26] Because peptoid (*N*-alkylglycyl) residues are imino acids by virtue of having side chains that are shifted from the α-carbon position to the N-position, there is no amide proton for forming intramolecular hydrogen bonds.[26] Peptoid-containing peptides have been reported to improve antibiotic cellular uptake and increase proteolytic stability and bioavailability.[22,27] It has been reported that peptoid-substituted AMPs have increased bacterial cell selectivity because of an altered bactericidal mechanism, consisting of an intracellular mode of action rather than a membrane targeting mechanism.[22,27]

Because papiliocin shows selectivity against Gram-negative bacteria and has poor antibacterial activity against Gram-positive bacteria, we designed potent broad-spectrum AMPs. Magainin shows moderate antibacterial activities against both Gram-negative and Gram-positive bacteria, while it does not show anti-inflammatory activities. In this study, we designed papiliocin−magainin 2 (PapMA) hybrid AMPs with proline in the hinge region to identify short antibiotic peptides with improved broad-spectrum antimicrobial activity and anti-inflammatory activities without cytotoxicity. We also designed a PapMA-k analogue by substituting a Lys peptoid residue for the Pro residue in PapMA, resulting in a different mechanism of action. We evaluated the antimicrobial activity and the cytotoxicity of the peptides, as well as permeabilization of model phospholipid membranes. To elucidate the role of bent structures provided by Pro and the peptoid on the bactericidal mechanism, we determined the tertiary structures of PapMA and PapMA-k in dodecylphosphocholine (DPC) micelles using NMR spectroscopy. Furthermore, we examined the anti-inflammatory effects of PapMA and PapMA-k in ultraviolet (UV)-irradiated human keratinocyte HaCaT cells and lipopolysaccharide (LPS)-stimulated macrophage RAW264.7 cells and confirmed that PapMA-k is a potent antibacterial agent as well as an anti-inflammatory agent and a skin photoaging agent lacking cytotoxicity. We also proved that PapMA-k is a cell-penetrating peptide while PapMA permeabilizes the bacterial cell membrane.

MATERIALS AND METHODS

Peptide Synthesis. Using *N*-(9-fluorenyl) methoxycarbonyl (Fmoc) chemistry, peptides were synthesized by solid-phase synthesis and purified as previously described.[22] Fmoc-Nlys (Boc) was synthesized as reported previously.[22] The peptide concentration was quantified using a UV spectrometer. The final purity of the peptides (>98%) was assessed by reverse-phase high-performance liquid chromatography (HPLC).

Antimicrobial Activity. *Bacillus subtilis* (KCTC 3068), *Enterococcus faecalis* (KCTC 2011), *Staphylococcus aureus* (KCTC 1621), *Salmonella typhimurium* (KCTC 1926), *Pseudomonas aeruginosa* (KCTC 1637), and *Escherichia coli* (KCTC 1682) were purchased from the Korean Collection for Type Cultures, Korea Research Institute of Bioscience and Biotechnology (Taejon, Korea). The clinical isolates of multidrug-resistant *P. aeruginosa* (MDRPA; CCARM 2002, 2095, and 2163), multidrug-resistant *E. coli* (MDREC; CCARM 1229 and 1238), multidrug-resistant *Acinetobacter baumannii* (MDRAB; CCARM 12035, 12036 and 12037), methicillin-resistant *Staphylococcus aureus* (MRSA; CCARM 3089, 3090, and 3126), and multidrug-resistant *S. typhimurium* (MDRST; CCARM 8003, 8007, and 8009) were provided by the Culture Collection of Antibiotic-Resistant Microbes (CCARM) at Seoul Women's University in Korea. Minimal inhibitory concentrations (MICs) of PapMA and PapMA-k against these bacteria were determined using a broth microdilution assay[28] and compared with those of papiliocin, magainin 2, and melittin. MIC values represent the lowest concentration of peptides that completely inhibit bacterial growth.

Hemolytic Activity. The hemolytic activity of the peptides was evaluated against human red blood cells (hRBCs) as previously reported.[13] The percent hemolysis was calculated using the equation

$$\text{hemolysis (\%)} = [(\text{OD}_{405}\ \text{sample} - \text{OD}_{405}\ \text{zero lysis}) / (\text{OD}_{405}\ 100\%\text{lysis} - \text{OD}_{405}\ \text{zero lysis})] \times 100$$

Cytotoxicity against Mammalian Cells. We measured the cytotoxicity against mouse macrophage-derived RAW264.7 cells and NIH-3T3 fibroblasts using a 3-(4,5-demethylthiazol-2-yl)-2,5-diphenyltetrazolium bromide (MTT) assay as previously described.[13]

Quantification of Nitrite Production in LPS-Stimulated RAW264.7 Cells. For nitric oxide (NO) production, the accumulation of nitrite in culture media was used as an indicator. RAW264.7 cells were seeded in 96-well culture plates at a density of 1×10^5 cells/mL. Cells were stimulated for 24 h with LPS (20 ng/mL) from *E. coli* O111:B4 (Sigma-Aldrich, St. Louis, MO) in the presence or absence of the peptides. As previously described, supernatants were collected and mixed with Griess reagent, followed by incubation at room temperature.[29] Via measurement of the absorbance at 540 nm, nitrite production was determined and converted to nitrite concentrations with reference to a standard curve generated using $NaNO_2$ concentrations.

Reverse Transcription Polymerase Chain Reaction (RT-PCR). Competitive RT-PCR was performed as previously described.[29] According to the manufacturer's instructions, an RNeasy kit (Qiagen, Hilden, Germany) was used for the extraction of total RNA; oligo(dT)-15 primers were used, and

DOI: 10.1021/acs.biochem.5b00392
Biochemistry 2015, 54, 3921−3931

Table 1. Amino Acid Sequences and Properties of PapMA and PapMA-k

	sequence	molecular weight	net charge[a]	hydrophilicity[b]	retention time (min)
papiliocin	RWKIFKKIEKVGRNVRDGIIKAGPAVAVVGQAATVVK-NH_2	4002.8	+8	0.28	23.41
magainin 2	GIGKFLHSAKKFGKAFVGEIMNS	2466.9	+3	0.02	28.96
PapMA	RWKIFKKIPKFLHSAKKF-NH_2	2302.7	+8	0.22	21.34
PapMA-k	RWKIFKKIkKFLHSAKKF-NH_2	2332.9	+9	0.39	19.96

[a]Net charge was calculated using the sum of each amino acid charge at pH 7.0. [b]Hydrophilicity is the total hydrophilicity (sum of the hydrophilicity indices of all residues) divided by the number of residues, according to the Hopp and Woods index.[39]

equal amounts of total RNA were reverse-transcribed into cDNA. PCR was performed using the same cycling conditions as described in our previous work.[29] Amplified PCR products were electrophoresed on 1% agarose gels and visualized using ethidium bromide staining.

UVB Irradiation Experiment. Human keratinocyte HaCaT cells were purchased from the ATCC (Manassas, VA). HaCaT cells were maintained in Dulbecco's modified Eagle's medium (DMEM) (Welgene, Daegu, Korea) supplemented with 10% FBS and 1% antibiotics. The medium was removed from the culture plates, and cells were washed twice with PBS and covered with a thin layer of PBS before UVB irradiation. Next, UVB irradiation was applied at a total energy dose of 40 mJ/cm^2. For the control, cells were washed with PBS only and not exposed to UV. Using a UVB Biolink BLX-312 spectrometer (Vilber Lourmat), the UVB light emits radiation in the range of 280−340 nm with peak emission at 314 nm. Once the cells were irradiated, they were further incubated in culture medium for various durations and collected using a cell scraper.

Interaction of PapMA and PapMA-k Analogues with FITC-Labeled LPS Aggregates. Samples were dissolved in 10 mM phosphate buffer (pH 6.0). Interaction of the peptide with FITC-conjugated LPS was studied by exciting 1 μg/mL FITC-LPS at 480 nm, and the change in FITC emission was monitored at 516 nm in the presence of different peptide concentrations.

Calcein Leakage Assay in Model Phospholipid Membranes. Calcein-entrapped large unilamellar vesicles (LUVs) mimicking human erythrocytes were composed of egg yolk L-α-phosphatidylcholine (EYPC) and cholesterol (CH) [10:1 (w/w)], whereas LUVs mimicking bacterial cell membranes were composed of EYPC and egg yolk L-α-phosphatidylglycerol (EYPG) [7:3 (w/w)]. LUVs were prepared as previously described.[29] Using the following equation, the percentage of dye leakage caused by hybrid peptides was calculated

$$\text{dye leakage}\ (\%) = 100 \times (F - F_0)/(F_t - F_0)$$

where F is the fluorescence intensity of peptide-treated vesicles, F_0 is the fluorescence intensity without the peptides, and F_t is the fluorescence intensity with Triton X-100.

Confocal Laser Scanning Microscopy. *E. coli* (KCTC 1682) cultures were grown to the mid log phase. *E. coli* cells at 10^7 colony-forming units (CFU)/mL in 10 mM PBS (pH 7.4) were incubated with 10 μg/mL FITC-labeled peptides for 30 min at 37 °C. Cells were washed with PBS and immobilized on a glass slide. An Olympus IX 70 confocal laser scanning microscope (Olympus, Tokyo, Japan) was used to obtain fluorescent images of peptides with a 488 nm band-pass filter for FITC excitation.

Circular Dichroism Analysis. Circular dichroism (CD) spectroscopy was used to study the secondary structures of peptides in the membrane-mimetic environments: water, 50% TFE/water solution, and 50 mM DPC micelles. Using a J810 spectropolarimeter (Jasco, Tokyo, Japan), the CD spectra of the peptides were recorded from 190 to 250 nm in 0.1 nm intervals with a 1 mm path length cell at 25 °C. For all CD experiments, the peptide concentration was 50 μM. Values from 10 scans were averaged for each spectrum and smoothed using J810 software.

NMR Experiments. The peptides at 1.0 mM were dissolved in 0.45 mL of an aqueous solution containing 150 mM DPC micelles (pH 5.4). To record a well-resolved spectrum in a membrane-mimetic environment, we determined the structure of papiliocin in DPC micelle. Because DPC micelles are model membranes, the peptide structure could differ from the actual structure in the bacterial cell membrane. Phase-sensitive two-dimensional experiments, including total correlation spectroscopy (TOCSY), nuclear Overhauser effect spectroscopy (NOESY), and double-quantum-filtered correlation spectroscopy (DQF-COSY), were performed as previously described.[29] For NOESY experiments, mixing times of 250 and 350 ms were used. Chemical shifts are referenced to the 4,4-dimethyl-4-silapentane-1-sulfonate (DSS) signal at 0 ppm. All NMR spectra were recorded on a Bruker 800 and 500 MHz spectrometer at the Korea Basic Science Institute (Ochang, Korea). NMR spectra were processed using NMRPipe[30] and visualized using Sparky.[31]

Structure Calculation. NOESY spectra recorded with mixing times of 250 and 150 ms were used to extract distance constraints. Depending on their distance range, all NOE intensities were divided into three classes: strong, 1.8−2.7 Å; medium, 1.8−3.5 Å; and weak, 1.8−5.0 Å. Standard pseudoatom corrections were applied as described previously.[22,32] XPLOR (version 3.851) was used to calculated peptide structures with the topology set as "topallhdg" and parameter set as "parallhdg". XPLO2D (version 2.1) was used to generate the parameters and topologies of lys peptoid.[22] The coordinates of the *trans* isomer of the Lys peptoid residue were built and minimized using XPLOR.[22] Structures were generated using a hybrid distance geometry-dynamical simulated annealing protocol.[22] One hundred structures were generated, and for further analysis, a total of 20 structures with the lowest energies were selected (BMRB accession numbers 21058 for PapMA and 21059 for *trans*-PapMA-k)

RESULTS

Peptide Design. Papiliocin has 37 amino acid residues and a net charge of +8; magainin 2 has 23 amino acid residues and a net charge of +3. We designed papiliocin−magainin 2 (PapMA) hybrid AMPs combining residues 1−8 of papiliocin and residues 4−12 of magainin 2 linked by a Pro residue. We also designed a PapMA-k analogue by substituting a Lys peptoid residue for the Pro residue in PapMA. The sequences and properties such as molecular weight and net charges of

DOI: 10.1021/acs.biochem.5b00392
Biochemistry 2015, 54, 3921−3931

PapMA and PapMA-k are listed in Table 1. Hybrid peptides are shorter (18 amino acid residues) than parent peptides. PapMA has a net charge of +8 and PapMA-k a net charge of +9. The hydrophilicity indices of papiliocin, magainin 2, PapMA, and PapMA-k were 0.28, 0.02, 0.22, and 0.39, respectively. We measured the hydrophobicity of the peptides by measuring retention times using a reversed-phase HPLC column. Retention times of papiliocin, magainin 2, PapMA, and PapMA-k were 23.41, 28.96, 21.34, and 19.96 min, respectively. PapMA-k is more hydrophilic than PapMA, as it contains a positively charged Lys peptoid residue in place of the Pro9 residue in PapMA.

Antimicrobial Activity. Antimicrobial activity was measured against three Gram-negative species (*S. typhimurium*, *E. coli*, and *P. aeruginosa*) and three Gram-positive species (*En. faecalis*, *B. subtilis*, and *St. aureus*). Antimicrobial activities of PapMA and PapMA-k were compared with those of papiliocin, magainin 2, and melittin. The geometric mean (GM) is the average value of the MIC values. A higher GM value indicates lower antimicrobial activity. PapMA and PapMA-k have MIC values comparable to that of melittin and GM values lower than those of papiliocin and magainin 2 (Table 2). The high GM value of papiliocin resulted from low antimicrobial activity against Gram-positive bacteria despite high antimicrobial activity against Gram-negative bacteria. These results showed that PapMA and PapMA-k had broad-spectrum antimicrobial activity compared with those of papiliocin and magainin 2.

Table 2. Hemolytic Activity and Antimicrobial Activity of PapMA and PapMA-k against Standard Bacterial Strains

	MIC[a] (μM)				
bacterial strain	papiliocin	magainin 2	PapMA	PapMA-k	melittin
E. coli	0.25	2.0	2.0	2.0	2.0
P. aeruginosa	1.0	8.0	4.0	4.0	4.0
S. typhimurium	0.5	16	2.0	4.0	8.0
B. subtilis	16	16	4.0	4.0	4.0
En. faecalis	64	16	16	16	2.0
St. aureus	32	16	4.0	4.0	8.0
GM[b]	19	12	5.3	5.7	4.7
MHC[c]	200	200	100	200	0.4
therapeutic index[d] (MHC/GM)	11	17	19	35	0.085

[a]Three independent experiments were performed in triplicate to measure MICs with a standard deviation of 14%. [b]The geometric means (GMs) of the MIC values measured for all six standard bacterial strains are shown. [c]The minimal peptide concentration produces hemolysis. When there is no detectable hemolysis observed at 100 μM, the therapeutic index was calculated using a value of 200 μM. [d]The therapeutic index is given as the ratio of the MHC to the geometric mean of the MIC. Larger values indicate greater cell selectivity.

We also examined the antimicrobial activity of the peptides against multidrug-resistant bacterial strains, as listed in Table 3. Average MIC values against Gram-negative and Gram-positive antibiotic-resistant bacteria were determined. Papiliocin showed strong antibacterial activity against Gram-negative antibiotic-resistant bacteria but showed a much higher GM value against Gram-positive antibiotic-resistant bacteria compared with those of both hybrid peptides. Magainin 2 showed antibacterial activities against Gram-negative antibiotic-resistant bacteria much lower than those of hybrid peptides. Both hybrid peptides displayed potent antibacterial activities against Gram-negative and Gram-positive antibiotic-resistant bacteria.

Hemolytic Activity and Cytotoxicity against Mammalian Cells. To check the cytotoxicity of PapMA and PapMA-k, we measured the hemolytic activities of PapMA and PapMA-k using human erythrocytes. The hemolytic activities of PapMA and PapMA-k are shown in Figure 1A. PapMA showed approximately 2% hemolytic activity at 100 μM, whereas PapMA-k showed no hemolytic activity, even at 100 μM. It has been reported that papiliocin and magainin 2 do not show hemolytic activity at 100 μM.[13,14]

We next checked the toxicities of PapMA and PapMA-k against RAW264.7 cells and NIH3T3 cells. We measured the mitochondrial reduction of MTT to a colored product by live cells to access the effect on cell growth. As shown in panels B and C of Figure 1, PapMA-k showed cytotoxicity against mammalian cells much lower than that of PapMA. The IC_{50} of PapMA-k was 42 μM against RAW264.7 cells, whereas the IC_{50} of PapMA was 10 μM. The IC_{50} of PapMA-k was 39 μM against NIH3T3 cells, while the IC_{50} of PapMA was 9 μM.

Inhibition of Nitrite (NO) Production in LPS-Stimulated RAW264.7 Cells. The outer membrane of Gram-negative bacteria is composed of LPS in the outer leaflet and phospholipids in the inner leaflet. In the outer leaflet, LPS is composed of hydrophilic *O*-antigen polysaccharide, core oligosaccharide, and lipid A. Lipid A is a lipid component of LPS. Gram-negative bacteria have a peptidoglycan layer between the outer membrane and inner cytoplasmic membrane. The release of LPS from bacteria leads to septic shock by inducing the production of a higher concentration of nitrite (NO) and pro-inflammatory cytokines. The effect of the peptides on anti-inflammatory activity was accessed by measuring the nitrite concentration in LPS-stimulated RAW264.7 macrophages. As shown in Figure 2, papiliocin significantly inhibited NO production while magainin 2 had no significant effect. However, PapMA and PapMA-k, hybrid peptides of papiliocin and magainin 2, inhibited NO production at 5.0−10 μM.

Inhibition of Inflammatory Cytokine Gene Expression in LPS-Stimulated RAW264.7 Cells. Expression of inflammatory cytokines, such as MIP-1, MIP-2, TNF-α, and IL-1β, in macrophages is induced by LPS. The effects of PapMA and PapMA-k on inflammatory cytokine gene expression in RAW264.7 cells stimulated with 20 ng/mL LPS were examined using RT-PCR. As shown in Figure 3, PapMA and PapMA-k suppressed inflammatory cytokine gene expression. In particular, PapMA-k strongly inhibited expression of the gene encoding inflammatory cytokines TNF-α and IL-1β compared with PapMA.

Inhibition of Inflammatory Cytokine Gene Expression in UVB-Irradiated HaCaT Cells. UV radiation damages human skin and causes conditions such as inflammation and photoaging.[33,34] Skin diseases are associated with upregulation of matrix metalloproteinase (MMP) and inflammatory cytokines in keratinocytes.[33,35] To investigate the effects of PapMA and PapMA-k on gene expression of inflammatory cytokines and MMP-1 in UVB-induced human keratinocyte cells, HaCaT cells were exposed to UVB (40 mJ/cm^2), and expression of MMP-1, TNF-α, and IL-6 was measured by RT-PCR. As shown in Figure 4, PapMA decreased the level of expression of MMP-1, TNF-α, and IL-6 by 61, 32, and 23%, respectively, compared with the UV-induced control. Also, PapMA-k decreased the level of expression of MMP-1, TNF-α, and IL-6 by 10, 18, and 20%, respectively, compared with the UV-induced control. PapMA displayed increased levels of

DOI: 10.1021/acs.biochem.5b00392
Biochemistry 2015, 54, 3921−3931

Table 3. Antimicrobial Activities of PapMA and PapMA-k against Antibiotic-Resistant Bacterial Strains

		MIC (μM)				
	bacterial strain	papiliocin	magainin 2	PapMA	PapMA-k	melittin
Gram-negative	MDRST 8003	4.0	32.0	4.0	4.0	8.0
	MDRST 8007	0.50	16.0	2.0	4.0	8.0
	MDRST 8009	0.50	16.0	2.0	4.0	8.0
	MDREC 1229	1.0	32.0	4.0	2.0	8.0
	MDREC 1238	2.0	16.0	2.0	4.0	8.0
	MDRPA 2002	1.0	16.0	2.0	8.0	4.0
	MDRPA 2095	2.0	16.0	2.0	8.0	4.0
	MDRPA 2163	2.0	16.0	2.0	8.0	4.0
	MDRAB 12035	1.0	16.0	2.0	8.0	4.0
	MDRAB 12036	1.0	16.0	2.0	8.0	4.0
	MDRAB 12037	1.0	16.0	2.0	8.0	4.0
	MDRAB 12005	2.0	32.0	2.0	4.0	4.0
	GM[a]	1.5	20.0	2.3	5.8	5.7
Gram-positive	MRSA 3089	>64	8.0	8.0	8.0	8.0
	MRSA 3108	>64	8.0	4.0	8.0	2.0
	MRSA 3126	>64	8.0	8.0	8.0	4.0
	GM[a]	>64	8.0	6.7	8.0	4.7

[a]The geometric means (GMs) of the MIC values from the tested antibiotic-resistant bacterial strains are listed.

inhibition of the inflammatory gene and cytokine expression compared with those of PapMA-k. Thus, PapMA and PapMA-k are candidate photoaging inhibitors.

FITC-Labeled LPS Aggregates. Interaction of AMPs with LPS can cause the dissociation of large LPS aggregates, resulting in an increase in fluorescence using FITC-conjugated LPS. Using this approach, we evaluated interaction of the peptide with LPS. As shown in Figure 5, peptide addition resulted in dose-dependent increases in FITC-LPS fluorescence, based on intensity changes in FITC-LPS fluorescence as a function of peptide concentration. These data suggest PapMA and PapMA-k as well as papiliocin interacted with LPS and dissociated larger LPS aggregates. In particular, papiliocin produced an increase in FITC-LPS fluorescence much larger than those produced by PapMA and PapMA-k, in accordance with antibacterial activities against Gram-negative bacteria and observed anti-inflammatory activity.

Peptide-Induced Permeabilization in Model Membranes. To investigate the mechanism underlying PapMA and PapMA-k activity, we measured the membrane permeabilizing potential of melittin, PapMA, and the peptoid analogue by monitoring the release of a fluorescent marker, calcein, from LUVs with different compositions. We employed negatively charged 7:3 (w/w) EYPC/EYPG LUVs and zwitterionic 10:1 (w/w) EYPC/CH LUVs. Membrane permeability was measured by the percentage of calcein leakage 2 min after addition of the peptide. Dose-dependent curves of peptide-induced calcein leakage shown in Figure 6 reveal that PapMA induces permeability of negatively charged vesicles, which mimic bacterial membranes more effectively than zwitterionic vesicles, suggesting that PapMA shows bacterial selectivity by targeting the bacterial cell membrane. Melittin showed strong leakage against both vesicles, suggesting that melittin is not bacterial cell selective. In contrast, PapMA-k produced <10% leakage from bacterial cell-mimetic, negatively charged vesicles at 10 μM. Thus, the relative abilities of PapMA-k to induce leakage from negatively charged vesicles did not correlate with its antimicrobial activities. This result suggests that PapMA-k functions via a different mechanism.

Confocal Laser Scanning Microscopy. To assess intracellular peptide localization, *E. coli* was incubated with FITC-labeled PapMA and PapMA-k and peptide distribution in bacteria was examined by confocal laser scanning microscopy. The antimicrobial activity of FITC-labeled peptides was evaluated, and it was identical to that of unlabeled peptides. FITC-labeled PapMA remained outside or on the cell membrane, whereas FITC-labeled PapMA-k penetrated the cell membrane and accumulated inside *E. coli* (Figure 7), suggesting that the cytoplasmic mechanism of action of PapMA-k could be related to inhibition of a particular intracellular function.

Circular Dichroism (CD) Measurements. CD experiments under various membranelike environments were performed to study the secondary structures of PapMA and PapMA-k. As shown in Figure S1 of the Supporting Information, PapMA and PapMA-k exhibited α-helical structures in 50 mM DPC micelles and 50% TFE/H_2O but displayed unordered structures in aqueous solution. PapMA and PapMA-k had two double minima at 205 and 220 nm, indicating that they adopted an α-helical structure under these membrane mimicking conditions.

Resonance Assignment and Structure Calculation of PapMA and PapMA-k. NMR experiments were performed in 150 mM DPC micelles. DPC micelles have been used to mimic zwitterionic membranes in structural studies of AMPs. Both proline and peptoid residues induce bent structures in α-helical structures of peptides.[22] The effect of peptoid substitution on structure was studied by sequence-specific assignments for PapMA and PapMA-k, mainly using DQF-COSY, TOCSY, and NOESY data. The chemical shifts of peptides in 150 mM DPC micelles at 303 K were referenced to 4,4-dimethyl-4-silapentane-1-sulfonate (DSS).

The NOESY spectra of PapMA in DPC micelles showed that the d$\alpha\delta(i+1)$ NOE for Ile^8-Pro^9 was observed while the d$\alpha\alpha(i+1)$ NOE for the *cis* isoform of proline was not observed, indicating that only a *trans* isoform exists for Pro^9 in DPC micelles. Figure 8 shows the NOESY spectra with the sequential assignments in the NH−CαH region for PapMA and PapMA-k. In contrast to PapMA, PapMA-k showed two

DOI: 10.1021/acs.biochem.5b00392
Biochemistry 2015, 54, 3921−3931

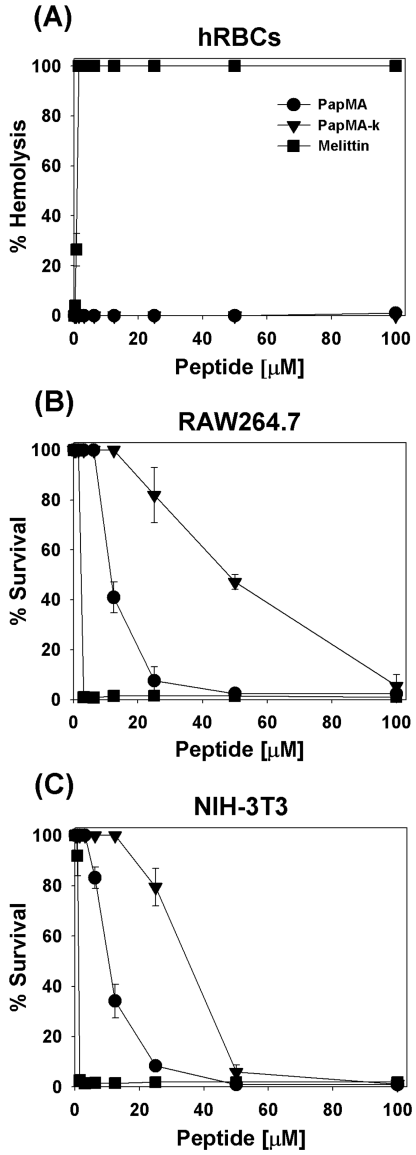

Figure 1. Dose–response curves of cytotoxicities of PapMA and PapMA-k vs (A) human red blood cells, (B) RAW264.7 cells, and (C) NIH3T3 cells. Peptides are represented by the following symbols: (●) PapMA, (▼) PapMA-k, and (■) melittin.

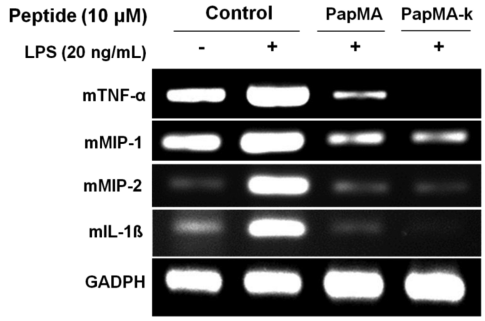

Figure 3. Effects of PapMA and PapMA-k on expression of inflammatory cytokines induced by LPS in RAW264.7 cells. Cells were stimulated without LPS (negative control) or with 20 ng/mL LPS in the absence or presence of peptide. Using RT-PCR, total RNA was analyzed for the expression of genes encoding TNF-α, IL-1β, MIP-1, MIP-2, and GAPDH (loading control).

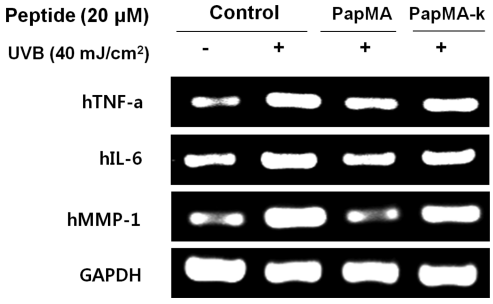

Figure 4. Effects of PapMA and PapMA-k on UVB-induced expression of MMP-1 and inflammatory cytokines in HaCaT cells. Using RT-PCR, total RNA was analyzed for the expression of genes encoding TNF-α, IL-6, MMP-1, and GAPDH (loading control).

sets of resonances for the *cis* isomer denoted by a black line and *trans* isomer denoted by a red line, indicating that PapMA-k existed in a dynamic equilibrium of a mixture of the *cis* and *trans* isomers. Because interconversion between two peptoid oligomer isomers is very slow, chemical shifts of two forms are resolved. The intensities of NOE peaks for the *trans* isomer of resonances in the NOESY spectra were much stronger than those of the *cis* isomer, as shown in Figure 8C. These results indicate that the population of *trans* isomer was much larger than those of the *cis* isomer. Figure S2 of the Supporting

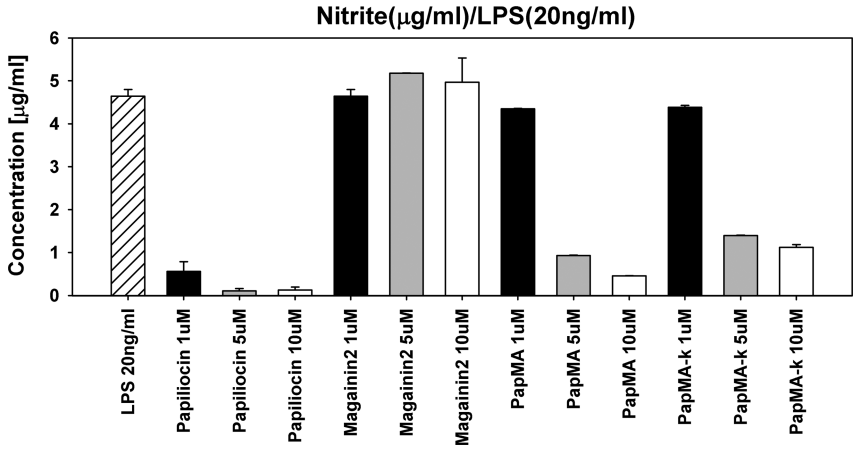

Figure 2. Anti-inflammatory activities of PapMA and PapMA-k. Inhibition of nitrite production by papiliocin, magainin 2, PapMA, and PapMA-k in RAW264.7 cells stimulated by LPS (20 ng/mL).

DOI: 10.1021/acs.biochem.5b00392
Biochemistry 2015, 54, 3921–3931

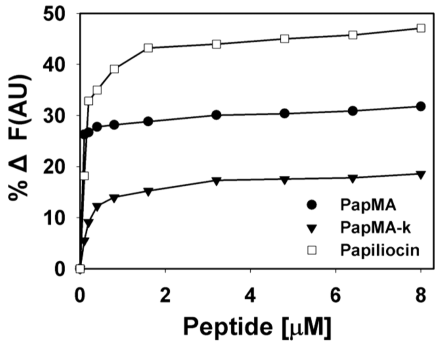

Figure 5. Intensity enhancement of FITC-labeled LPS as a function of PapMA and PapMA-k concentration.

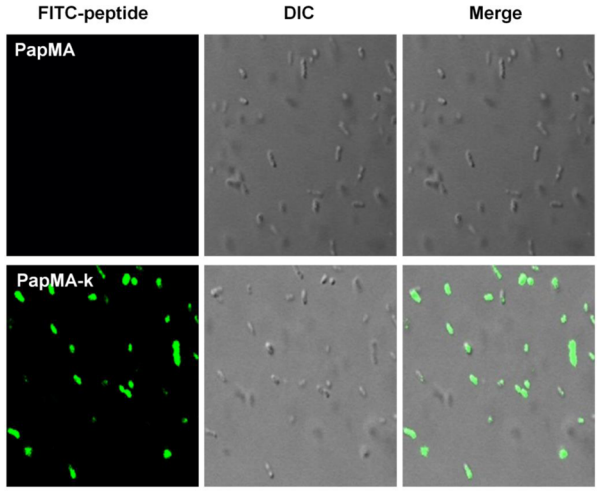

Figure 7. Confocal fluorescence microscopic images of *E. coli* cells. *E. coli* cells were incubated with FITC-labeled PapMA and PapMA-k at a concentration of 10 μg/mL for 30 min at 37 °C. The right panels represent a normal image of the bacteria, while the left panels represent laser scanning images of FITC-labeled peptides.

Information shows the NOE contacts for the two isomers of PapMA-k. In the *trans* isomer (Figure S2A of the Supporting Information), the side chain of Nlys[9] shows many NOEs with an Ile[8] side chain. In the *cis* isomer, NOEs were not observed between the Nlys[9] side chain and the Ile[8] side chain. As shown Figure S2B of the Supporting Information, the Ile[8] side chain in the *cis* isomer severely conflicted with the Lys[10] side chain, resulting in a small population of the PapMA-k *cis* isomer. Because the *trans* isomer is the major form of PapMA-k without steric hindrance and the *cis* isomer gave very weak NOEs, we determined the tertiary structure of only the PapMA-k *trans* isomer.

As shown in Figure S3 of the Supporting Information, nonsequential NOE connectivities characteristic of an α-helical structure, such as dαN(i,i+3) and dαN(i,i+4), were observed in the C-terminal region of both peptides. The ^{1}H chemical shift index was calculated using the method of Wishart and colleagues;[36] a dense grouping of four or more −1 values not interrupted by a +1 value suggests the presence of an α-helical structure in this region.

Sequential ($|i - j| = 1$), medium-range ($1 < |i - j| \leq 5$), and long-range ($|i - j| > 5$) distances, hydrogen bonding, and torsion angle limitations were used as experimental constraints for PapMA and PapMA-k structure calculation. We accepted structures with only small deviations from the experimental constraints and the idealized covalent geometry as previously described.[29] We then analyzed 20 output structures having the lowest energy. Panels A and C of Figure 9 show the average structure of PapMA and *trans*-PapMA-k, respectively. Panels B and D of Figure 9 show the superimposition of the backbones of the final 20 lowest-energy structures of PapMA and *trans*-PapMA-k, respectively. The root-mean-square deviations (rmsd's) from an idealized geometry for bond lengths and angles of PapMA and *trans*-PapMA-k are 0.005 Å and 0.732° and 0.004 Å and 1.947°, respectively. No structures had violations larger than 0.5 Å from the NOE distance constraints or 3° from dihedral angle constraints. All structures exhibited good covalent geometry. As listed in Table 4, superimposition of the backbones of the 20 lowest-energy structures from residue Lys[10] to Lys[17] of PapMA and *trans*-PapMA-k showed that the rms deviations from the mean structure were 0.37 ± 0.13 and 0.44 ± 0.15 Å for the backbone atoms (N, Cα, C′, and O) and 1.56 ± 0.38 and 1.69 ± 0.33 Å for all heavy atoms, respectively (BMRB accession numbers 21058 for PapMA and 21059 for *trans*-PapMA-k).

PapMA has a bent structure at Pro[9], an α-helix from Lys[3] to Lys[7], and another one from Lys[10] to Lys[17]. Nlys[9] in PapMA-k forms a hinge that is more flexible than the hinge in PapMA, resulting in the two conformers. The *trans* form of PapMA-k also has an α-helix from Lys[3] to Lys[7] and one from Lys[10] to Lys[17]. This result suggests that this flexible hinge at the central

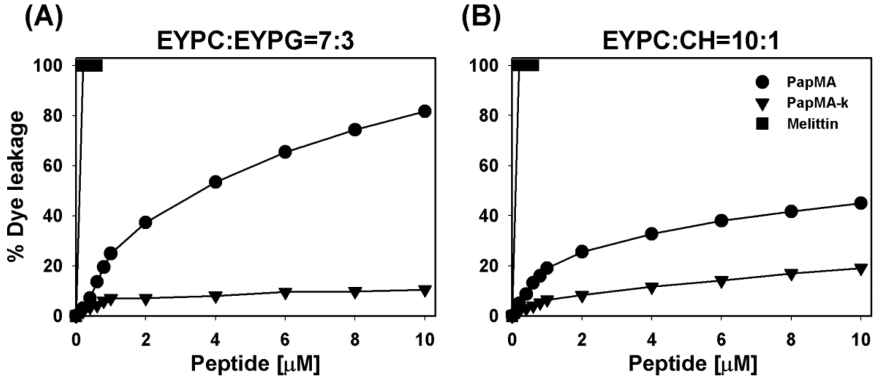

Figure 6. Dose-dependent curves showing dye leakage from (A) EYPC/EYPG [7:3 (w/w)] and (B) EYPC/CH [10:1 (w/w)] LUVs induced by PapMA, PapMA-k, and melittin. To monitor the leakage of calcein from LUVs, the fluorescence intensity was measured using an excitation wavelength of 490 nm and an emission wavelength of 520 nm.

DOI: 10.1021/acs.biochem.5b00392
Biochemistry 2015, 54, 3921−3931

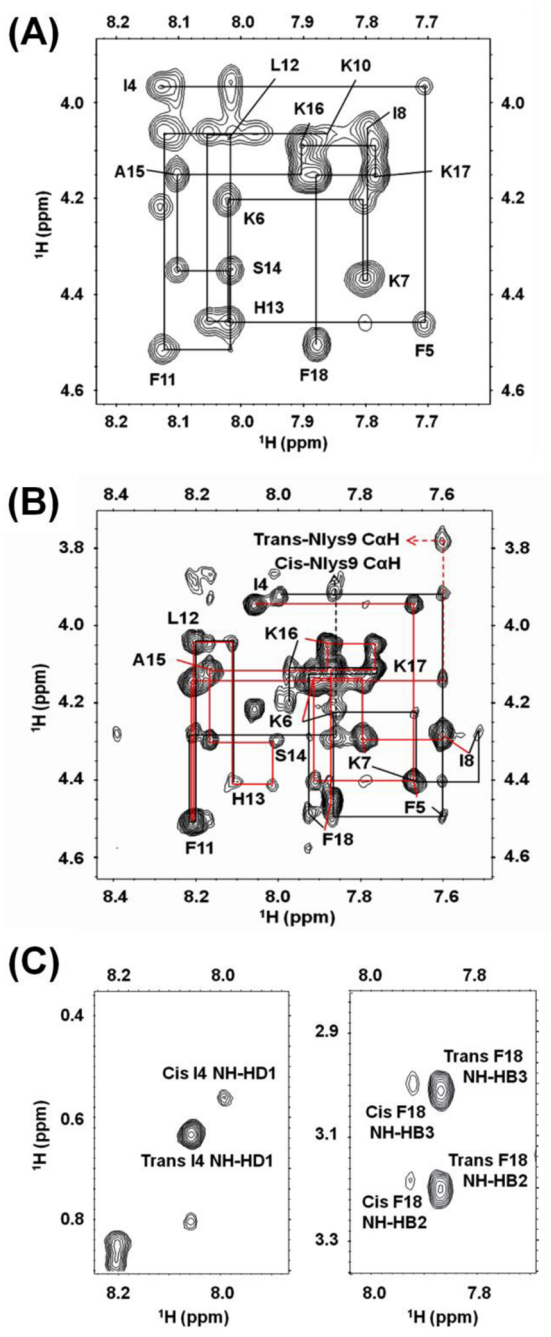

Figure 8. NOESY spectra of the NH−CαH region of (A) PapMA and (B) PapMA-k in 150 mM DPC micelles at pH 5.5 and 303 K. PapMA-k existed in two conformers; the red line shows data for *trans*-PapMA-k and the line those for *cis*-PapMA-k. (C) NOESY spectra of the side chain region of PapMA-k showing the relative intensity of *trans*-PapMA-k and *cis*-PapMA-k.

region of PapMA-k is important for penetrating the bacterial cell membrane and conferring high bacterial cell selectivity.

DISCUSSION

In this study, we evaluated the antimicrobial and anti-inflammatory activity of hybrid peptides of papiliocin and magainin 2. PapMA and PapMA-k showed high broad-spectrum antibacterial activity compared with that o papiliocin. Cytotoxicity correlated with peptide hydrophobicity. We measured the retention time of PapMA and PapMA-k by reverse-phase HPLC. PapMA-k was less hydrophobic than PapMA because of the positively charged peptoid residue in the hinge region. The retention time was 21.34 min for PapMA and 19.96 min for PapMA-k (Table 1). The less hydrophobic PapMA-k peptide displayed decreased cytotoxicity and increased bacterial cell selectivity. PapMA exhibited high cytotoxicity to mammalian cells, but PapMA-k was much less cytotoxic than PapMA. In peptoid residues, the side chain was shifted from the α-carbon atom to the nitrogen atom.[26] This characteristic is useful for designing AMPs with high bacterial cell selectivity.[22,27] In our previous study, Lys peptoid-substituted Pis-1 (Pis-1[NkG]) decreased cytotoxicity and increased bacterial cell selectivity compared with those seen with Pis-1 and Pis-1 [PG] substituted for the Pro residue.[22]

The therapeutic index represents the ratio of the minimally effective concentration toward human red blood cells and the minimally inhibitory concentration against bacteria. A high therapeutic index indicates higher antimicrobial activity with lower cytotoxicity against mammalian cells. The therapeutic indices of PapMA and PapMA-k were 19 and 35, respectively, as listed in Table 2. These values were higher than the value of either melittin (0.085) or papiliocin.[13] The GM value represents the average of the MIC values. The MICs of papiliocin against antibiotic-resistant Gram-negative and Gram-positive bacteria were 1.5 and >64, respectively, indicating that papiliocin had more effective antimicrobial activity against Gram-negative bacteria. However, the values of PapMA and PapMA-k against antibiotic-resistant Gram-positive bacteria were 6.7 and 8, respectively. Hybrid peptides resulted in improved antimicrobial activity against Gram-positive bacteria compared with that of papiliocin, showing that hybrid peptides have enhanced broad-spectrum antimicrobial activity.

Gram-negative bacteria possess outer membranes containing phospholipids, proteins, and an LPS layer. LPS release in living organisms causes various physiological effects, such as fever and generalized inflammation.[37] We investigated the anti-inflammatory activity of PapMA and PapMA-k. PapMA and PapMA-k inhibited NO production more effectively than magainin 2 did. PapMA and PapMA-k also suppressed production of inflammatory cytokines, including TNF-α, IL-1β, MIP-1, and MIP-2. To investigate the interaction between the peptides and LPS, we measured the increase in fluorescence intensity by dissociation of FITC-LPS aggregates. PapMA caused an increased level of dissociation of large FITC-LPS aggregates into smaller sizes compared with PapMA-k, suggesting a stronger interaction between PapMA and LPS.

To investigate the mechanism, we measured membrane permeabilizing ability by monitoring the increase in the escaped fluorescence intensity. PapMA induced a high level of leakage of calcein from negatively charged bacterial membrane mimic vesicles, indicating that PapMA selectively targets bacterial membranes. In contrast, PapMA-k showed <10% leakage of the fluorescent dye at 10 μM compared with 80% leakage for PapMA, suggesting that PapMA-k may have a different bactericidal mechanism. We assessed the intracellular localization of the peptides using confocal laser scanning microscopy, which revealed that PapMA-k, featuring a Lys peptoid-substituted peptide at the hinge, penetrated the bacterial cell membrane and accumulated inside *E. coli*, whereas PapMA, featuring a proline residue-substituted peptide at the hinge, remained on the cell membrane.

This research provided the structures of PapMA and Lys peptoid-substituted PapMA-k in a membrane mimic environ-

DOI: 10.1021/acs.biochem.5b00392
Biochemistry 2015, 54, 3921−3931

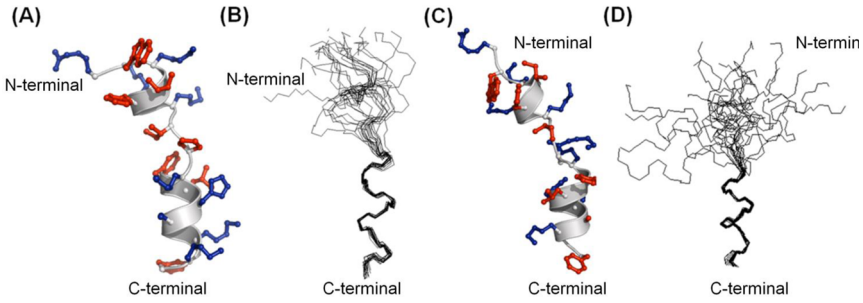

Figure 9. (A) Ribbon diagram of the lowest-energy structure of PapMA in 150 mM DPC micelles. (B) Superimposition of the 20 lowest-energy structures of PapMA. (C) Ribbon diagram of the lowest-energy structure of *trans*-PapMA-k in 150 mM DPC micelles. (D) Superimposition of the 20 lowest-energy structures of *trans*-PapMA-k. The hydrophobic residues are colored red and the hydrophilic residues blue.

Table 4. Structural Statistics and Mean Pairwise Root-Mean-Square Deviations for the 20 Lowest-Energy Structures of PapMA and *trans*-PapMA-k in 150 mM DPC Micelles at 303 K[a]

	PapMA	*trans*-PapMA-k
no. of experimental distance constraints		
total	296	175
sequential	160	107
medium-range	136	68
intraresidue	0	0
hydrogen bond constraints	6	6
dihedral angle constraints	14	15
rmsd from experimental geometry		
NOE (Å)	0.044 ± 0.00	0.023 ± 0.01
f (deg)	0.709 ± 0.34	0.429 ± 0.22
rmsd from covalent geometry		
bonds (Å)	0.005 ± 0.00	0.004 ± 0.00
angles (deg)	0.732 ± 0.02	1.947 ± 0.01
impropers (deg)	0.657 ± 0.08	1.508 ± 0.01
average energies (kcal mol^{-1})		
E_{tot}	126.38 ± 10.58	503.01 ± 9.61
E_{NOE}	29.26 ± 5.54	4.78 ± 2.90
E_{tor}	0.44 ± 0.49	0.19 ± 0.31
E_{repel}	20.31 ± 5.25	5.37 ± 3.16
rmsd from the mean structure		
backbone atoms of residues 10−17	0.37 ± 0.13	0.44 ± 0.15
all heavy atoms of residues 10−17	1.56 ± 0.38	1.69 ± 0.33
backbone atoms of residues 2−8	0.11 ± 0.05	0.53 ± 0.30
all heavy atoms of residues 2−8	0.95 ± 0.20	2.13 ± 0.45

[a] E_{NOE}, E_{tor}, and E_{repel} are the energies explained in our previous paper.[29] The rmsd values were calculated by best fitting the coordinates of the backbone heavy atoms for all residues of the 20 converged structures. The numbers given for the backbone atoms and all heavy atoms represent means ± standard deviations.

ment. The amphipathicity is important for incorporating into bacterial cell membranes by interacting between the membrane lipid and hydrophobic faces of peptides.[38] In our previous paper, papiliocin showed two α-helical structures, N-terminal amphipathic helix and hydrophobic C-terminal helix.[13] The N-terminal helix region of papiliocin is important for its activities. Magainin 2 is a linear amphipathic α-helical structure. PapMA consisted of a single *trans* conformer with a rigid proline hinge region, whereas PapMA-k existed in an equilibrium of *trans* and *cis* isomers with a flexible hinge region. Peptoid residues break α-helical structures by forming a β-turn. PapMA-k displayed a flexible hinge structure at Nlys[9] in DPC micelles. Penetration into bacterial cell membranes and accumulation in the cytoplasm could be facilitated by the structural flexibility of the peptoid-containing PapMA-k peptide, conferred by the dynamic equilibrium between the two isomers; the chemical properties of the Lys peptoid residue itself confer this ability. This flexible structure as well as the positively charged Lys peptoid residue plays important roles in bacterial cell selectivity in PapMA-k. Conversely, PapMA displayed a rigid bent structure conferred by proline and did not penetrate the bacterial cell membrane.

Photoaging and skin damage, such as wrinkles and pigmentation, can be caused by exposure to UVB irradiation.[33−35] Members of the MMP family are zinc-dependent endopeptidases that include MMP-1, MMP-3, and MMP-9.[35] MMPs play a critical role in the degradation of the basement membrane and extracellular matrix, as well as in the expression of inflammatory cytokines that influence the aging process.[34,35] Inflammation mediated by these cytokines increases the level of production of ROS and additional cytokines, thus amplifying the effect of UV exposure.[33] PapMA and PapMA-k suppressed gene expression of MMP-1 and inflammatory cytokines,

DOI: 10.1021/acs.biochem.5b00392
Biochemistry 2015, 54, 3921−3931

including TNF-a and IL-6, suggesting that PapMA and PapMA-k have the potential to protect against photoaging.

In conclusion, the hybrid peptides PapMA and PapMA-k displayed antimicrobial activity against both Gram-negative and Gram-positive bacteria compared with parent peptides and had amino acid sequences shorter than those of papiliocin and magainin 2. Thus, PapMA and PapMA-k are promising antimicrobial candidates for the treatment of infections involving standard and antibiotic-resistant bacteria, endotoxic shock, and antiaging by UVB irradiation. Because PapMA-k was a cell-penetrating peptide, further studies will elucidate the intracellular targeting mechanisms of peptoid-containing peptides.

■ ASSOCIATED CONTENT

Supporting Information

Figures S1−S3. The Supporting Information is available free of charge on the ACS Publications website at DOI: 10.1021/acs.biochem.5b00392.

■ AUTHOR INFORMATION

Corresponding Author

*Department of Bioscience and Biotechnology, Konkuk University, Seoul 143-701, South Korea. Phone: +82-(0)2-450-3421. Fax: +82-(0)2-447-5987. E-mail: ymkim@konkuk.ac.kr.

Funding

This work was supported by a grant from Konkuk University.

Notes

The authors declare no competing financial interest.

■ ABBREVIATIONS

AMP, antimicrobial peptide; CD, circular dichroism; LPS, lipopolysaccharide; LUV, large unilamellar vesicle; SUV, small unilamellar vesicle; NMR, nuclear magnetic resonance; DPC, dodecylphosphocholine; FITC, fluorescein isothiocyanate; NOESY, nuclear magnetic resonance; TOCSY, total correlation spectroscopy; DQF-COSY, double-quantum-filtered correlation spectroscopy.

■ REFERENCES

(1) Hancock, R. E., and Sahl, H. G. (2006) Antimicrobial and host-defense peptides as new anti-infective therapeutic strategies. *Nat. Biotechnol. 24*, 1551−1557.

(2) Andreu, D., and Rivas, L. (1998) Animal antimicrobial peptides: An overview. *Biopolymers 47*, 415−433.

(3) Zasloff, M. (1992) Antibiotic peptides as mediators of innate immunity. *Curr. Opin. Immunol. 4*, 3−7.

(4) Nijnik, A., and Hancock, R. (2009) Host defence peptides: Antimicrobial and immunomodulatory activity and potential applications for tackling antibiotic-resistant infections. *Emerging Health Threats Journal 2*, e1.

(5) Brogden, K. A. (2005) Antimicrobial peptides: Pore formers or metabolic inhibitors in bacteria? *Nat. Rev. Microbiol. 3*, 238−250.

(6) Shai, Y. (2002) Mode of action of membrane active antimicrobial peptides. *Biopolymers 66*, 236−248.

(7) Blondelle, S. E., Lohner, K., and Aguilar, M. (1999) Lipid-induced conformation and lipid-binding properties of cytolytic and antimicrobial peptides: Determination and biological specificity. *Biochim. Biophys. Acta 1462*, 89−108.

(8) Hancock, R. E., and Rozek, A. (2002) Role of membranes in the activities of antimicrobial cationic peptides. *FEMS Microbiol. Lett. 206*, 143−149.

(9) Dathe, M., and Wieprecht, T. (1999) Structural features of helical antimicrobial peptides: Their potential to modulate activity on model membranes and biological cells. *Biochim. Biophys. Acta 1462*, 71−87.

(10) Kim, S. R., Hong, M. Y., Park, S. W., Choi, K. H., Yun, E. Y., Goo, T. W., Kang, S. W., Suh, H. J., Kim, I., and Hwang, J. S. (2010) Characterization and cDNA cloning of a cecropin-like antimicrobial peptide, papiliocin, from the swallowtail butterfly, *Papilio xuthus*. *Mol. Cells 29*, 419−423.

(11) Lee, J., Hwang, J. S., Hwang, B., Kim, J. K., Kim, S. R., Kim, Y., and Lee, D. G. (2010) Membrane Perturbation Induced by Papiliocin Peptide, Derived from *Papilio xuthus*, in *Candida albicans*. *J. Microbiol. Biotechnol. 20*, 1185−1188.

(12) Lee, J., Hwang, J. S., Hwang, B., Kim, J. K., Kim, S. R., Kim, Y., and Lee, D. G. (2010) Influence of the papiliocin peptide derived from *Papilio xuthus* on the perturbation of fungal cell membranes. *FEMS Microbiol. Lett. 311*, 70−75.

(13) Kim, J. K., Lee, E., Shin, S., Jeong, K. W., Lee, J. Y., Bae, S. Y., Kim, S. H., Lee, J., Kim, S. R., Lee, D. G., Hwang, J. S., and Kim, Y. (2011) Structure and function of papiliocin with antimicrobial and anti-inflammatory activities isolated from the swallowtail butterfly, *Papilio xuthus*. *J. Biol. Chem. 286*, 41296−41311.

(14) Zasloff, M. (1987) Magainins, a class of antimicrobial peptides from *Xenopus* skin: Isolation, characterization of two active forms, and partial cDNA sequence of a precursor. *Proc. Natl. Acad. Sci. U.S.A. 84*, 5449−5453.

(15) Maloy, W. L., and Kari, U. P. (1995) Structure-activity studies on magainins and other host defense peptides. *Biopolymers 37*, 105−122.

(16) Shin, S. Y., Lee, M. K., Kim, K. L., and Hahm, K. S. (1997) Structure-antitumor and hemolytic activity relationships of synthetic peptides derived from cecropin A-magainin 2 and cecropin A-melittin hybrid peptides. *J. Pept. Res. 50*, 279−285.

(17) Shin, S. Y., Kang, J. H., Lee, M. K., Kim, S. Y., Kim, Y., and Hahm, K. S. (1998) Cecropin A-magainin 2 hybrid peptides having potent antimicrobial activity with low hemolytic effect. *Biochem. Mol. Biol. Int. 44*, 1119−1126.

(18) Oh, D., Shin, S. Y., Kang, J. H., Hahm, K. S., Kim, K. L., and Kim, Y. (1999) NMR structural characterization of cecropin A(1−8)-magainin 2(1−12) and cecropin A (1−8)-melittin (1−12) hybrid peptides. *J. Pept. Res. 53*, 578−589.

(19) Shin, S. Y., Kang, J. H., and Hahm, K. S. (1999) Structure-antibacterial, antitumor and hemolytic activity relationships of cecropin A-magainin 2 and cecropin A-melittin hybrid peptides. *J. Pept. Res. 53*, 82−90.

(20) Shin, S. Y., Kang, J. H., Jang, S. Y., Kim, Y., Kim, K. L., and Hahm, K. S. (2000) Effects of the hinge region of cecropin A(1−8)-magainin 2(1−12), a synthetic antimicrobial peptide, on liposomes, bacterial and tumor cells. *Biochim. Biophys. Acta 1463*, 209−218.

(21) Oh, D., Shin, S. Y., Lee, S., Kang, J. H., Kim, S. D., Ryu, P. D., Hahm, K. S., and Kim, Y. (2000) Role of the hinge region and the tryptophan residue in the synthetic antimicrobial peptides, cecropin A(1−8)-magainin 2(1−12) and its analogues, on their antibiotic activities and structures. *Biochemistry 39*, 11855−11864.

(22) Kim, J. K., Lee, S. A., Shin, S., Lee, J. Y., Jeong, K. W., Nan, Y. H., Park, Y. S., Shin, S. Y., and Kim, Y. (2010) Structural flexibility and the positive charges are the key factors in bacterial cell selectivity and membrane penetration of peptoid-substituted analog of Piscidin 1. *Biochim. Biophys. Acta 1798*, 1913−1925.

(23) Park, C. B., Yi, K. S., Matsuzaki, K., Kim, M. S., and Kim, S. C. (2000) Structure-activity analysis of buforin II, a histone H2A-derived antimicrobial peptide: The proline hinge is responsible for the cell-penetrating ability of buforin II. *Proc. Natl. Acad. Sci. U.S.A. 97*, 8245−8250.

(24) Lee, J. K., Gopal, R., Park, S. C., Ko, H. S., Kim, Y., Hahm, K. S., and Park, Y. (2013) A proline-hinge alters the characteristics of the amphipathic α-helical AMPs. *PLoS One 8*, e67597.

(25) Bobone, S., Bocchinfuso, G., Park, Y., Palleschi, A., Hahm, K. S., and Stella, L. (2013) The importance of being kinked: Role of Pro

DOI: 10.1021/acs.biochem.5b00392
Biochemistry 2015, 54, 3921−3931

residues in the selectivity of the helical antimicrobial peptide P5. *J. Pept. Sci. 19*, 758−769.
(26) Simon, R. J., Kania, R. S., Zuckermann, R. N., Huebner, V. D., Jewell, D. A., Banville, S., Ng, S., Wang, L., Rosenberg, S., Marlowe, C. K., et al. (1992) Peptoids: A modular approach to drug discovery. *Proc. Natl. Acad. Sci. U.S.A. 89*, 9367−9371.
(27) Zuckermann, R. N., and Kodadek, T. (2009) Peptoids as potential therapeutics. *Curr. Opin. Mol. Ther. 11*, 299−307.
(28) Lee, J., Jeong, K. W., Shin, S., Lee, J., and Kim, Y. (2012) Discovery of novel selective inhibitors of *Staphylococcus aureus* β-ketoacyl acyl carrier protein synthase III. *Eur. J. Med. Chem. 47*, 261−269.
(29) Lee, E., Kim, J. K., Shin, S., Jeong, K. W., Shin, A., Lee, J., Lee, D. G., Hwang, J. S., and Kim, Y. (2013) *Biochim. Biophys. Acta 1828*, 271−283.
(30) Delaglio, F., Grzesiek, S., Vuister, G. W., Zhu, G., Pfeifer, J., and Bax, A. (1995) NMRPipe: A multidimensional spectral processing system based on UNIX pipes. *J. Biomol. NMR 6*, 277−293.
(31) Goddard, T. D., and Kneller, D. G. (2002) *Sparky 3*, University of California, San Francisco.
(32) Wuthrich, K., Billeter, M., and Braun, W. (1983) Pseudo-structures for the 20 common amino acids for use in studies of protein conformations by measurements of intramolecular proton-proton distance constraints with nuclear magnetic resonance. *J. Mol. Biol. 169*, 949−961.
(33) Chiang, H. M., Chiu, H. H., Liao, S. T., Chen, Y. T., Chang, H. C., and Wen, K. C. (2013) Isoflavonoid-Rich *Flemingia macrophylla* Extract Attenuates UVB-Induced Skin Damage by Scavenging Reactive Oxygen Species and Inhibiting MAP Kinase and MMP Expression. *J. Evidence-Based Complementary Altern. Med. 2013*, 696879.
(34) Choi, H. K., Kim, D. H., Kim, J. W., Ngadiran, S., Sarmidi, M. R., and Park, C. S. (2010) *Labisia pumila* extract protects skin cells from photoaging caused by UVB irradiation. *J. Biosci. Bioeng. 109*, 291−296.
(35) Kim, J. K., Mun, S., Kim, M. S., Kim, M. B., Sa, B. K., and Hwang, J. K. (2012) 5,7-Dimethoxyflavone, an activator of PPARα/γ, inhibits UVB-induced MMP expression in human skin fibroblast cells. *Exp. Dermatol. 21*, 211−216.
(36) Wishart, D. S., Sykes, B. D., and Richards, F. M. (1992) The chemical shift index: A fast and simple method for the assignment of protein secondary structure through NMR spectroscopy. *Biochemistry 31*, 1647−1651.
(37) Alexander, C., and Rietschel, E. T. (2001) Bacterial lipopolysaccharides and innate immunity. *J. Endotoxin Res. 7*, 167−202.
(38) Giangaspero, A., Sandri, L., and Tossi, A. (2001) Amphipathic α helical antimicrobial peptides. *Eur. J. Biochem. 268*, 5589−5600.
(39) Hopp, T. P., and Woods, K. R. (1981) Prediction of protein antigenic determinants from amino acid sequences. *Proc. Natl. Acad. Sci. U.S.A. 78*, 3824−3828.

DOI: 10.1021/acs.biochem.5b00392
Biochemistry 2015, 54, 3921−3931